OBSERVATION ERROR MODELING AND ENKF OSSES EXAMINING THE IMPACT OF SPATIAL AND TEMPORAL RESOLUTIONS AND ERRORS OF PHASED-ARRAY RADAR

Y. Umemoto[1,*], T. Lei[2], T.-Y. Yu[1], and M. Xue[2,3]

[1] School of Electrical and Computer Engineering
[2] Center for Analysis and Prediction of Storms (CAPS)
[3] School of Meteorology
The University of Oklahoma, Norman, U.S.A.

1. INTRODUCTION

The S-band Phased Array Radar (PAR) at the National Weather Radar Testbed (NWRT) in Norman, Oklahoma can adaptively scan multiple regions of interest and provide rapidly updated weather observations by electronically beam steering. This capability allows providing fast updates of weather information with high statistical accuracy with scanning strategy termed beam multiplexing ([Yu et al., 2007]). Since PAR has wider beams ($\sim 2°$) than that of the operational WSR-88D ($\sim 1°$), PAR has lower spatial resolutions at far ranges.

Among efforts to better realize its potential for improving convective-storm analysis and prediction, an EnKF system developed for the Advanced Regional Prediction System (ARPS) has recently been enhanced to assimilate radar data radial by radial, with proper beam pattern weighting functions in all three directions. This capability allows us to take advantage of the range and azimuthal over-sampling capabilities of PAR radar data, and the ability for PAR to can gain better accuracy through beam multiplexing.

In this study, the impact of assimilation of data observed with various scanning strategies generated in Observing System Simulation Experiments (OSSEs, e.g., [Snyder et al., 2003]; [Zhang et al., 2004]; [Tong and Xue , 2005], TX05 hereafter; [Xue et al., 2006], TXD06 hereafter; [Jung et al., 2008]; [Lei et al., 2007], L07 hereafter) in a storm scale numerical weather prediction model using the Ensemble Kalman Filter (EnKF) on the analysis of storms is examined. In addition to that, earlier OSSEs assimilating data using EnKF are extended to take into account of spatially inhomogeneous and scan-interval-dependent observation error estimates. Through proper modeling the expected error in the observations collected using different scanning strategies, the results of the OSSEs become more realistic, and an optimal combination of the spatial and temporal resolutions and data precision is sought through the EnKF OSSEs. The special and scan interval-dependent observation errors are estimated using parameters produced from simulated radar waveforms. Preliminary results are presented.

* *Corresponding author address:* Yasuko Umemoto, University of Oklahoma, School of Meteorology, 120 David L. Boren Blvd., Rm 4638, Norman, OK 73072-7307; e-mail: yasuko@ou.edu

This paper is organized as follows: in section 2, simulated radar data, the observational error models OSSE experimental design and the specification of the ARPS EnKF system are described. Preliminary results are presented in section 3 and discussions are given in section 4.

2. ERROR MODELS AND EXPERIMENTAL DESIGN

2.1. EnKF system and simulated radar observations

In this experiment, the perfect model is assumed, and the same model and exactly the same configurations are used for the truth simulation and ensemble forecasts. The same observation operator is used in EnKF analysis and simulation of observation. The ARPS EnKF system used in this study is based on TX05, XTD06, and L07 including the ability to assimilate radar observations radial by radial in their native radar coordinates, which allows examining impact of various scanning strategies including over-sampling.

Though the NWRT PAR has a range resolution spacing of 250 m, simulated observations in this study has a range spacing that is no smaller than the grid interval of the truth simulation (1 km in horizontal).

The range weighting function, $W(r)$ is applied within the radar sampling volume as follows:

$$W(r_{i,j,k}) = \begin{cases} 1 & |r_{i,j,k} - r_0| \le ar_6 \\ W_t(|r_{i,j,k} - r_0| - ar_6) & |r_{i,j,k} - r_0| > ar_6 \end{cases} \quad (1)$$

where a is 1.5 for this experiment and W_t is given as follows (Eq. (11.118) of [Doviak abd Zrnic , 1993]):

$$|W_t(dr)|^2 = exp[-(dr)^2/2{\sigma_r}^2] \quad (2)$$

where

$${\sigma_r}^2 = (0.30r_6)^2 \quad (3)$$

as Eq. (5.76) of [Doviak abd Zrnic , 1993] and r_6 is taken as 235 m as in [Wood and Brown , 1997]. The azimuth and elevation weighting functions are applied as follows ([Wood

and Brown , 1997]):

$$f^4(\theta_{i,j,k},\phi_{i,j,k}) = exp\left\{-4ln4\left[\left(\frac{\theta_{i,j,k}-\theta}{\theta_w}\right)^2+\left(\frac{\phi_{i,j,k}-\phi}{\phi_w}\right)^2\right]\right\} \quad (4)$$

where θ_w and ϕ_w are beam width in azimuth and elevation respectively.

2.2. Error models

The EnKF data assimilation method is based on the basic assumptions of Gaussian distributions of both background forecast and observation errors. In OSSEs, radar observations are created by adding random noise to the error-free observations. TX05 and XTD06 simulated reflectivity observation errors by adding noise to the simulated reflectivity that has a Gaussian distribution of zero mean and a standard deviation (SD) of 5 dBZ for all radar data L07 used SDs of 2 dBZ and 1 m/s for error estimation of reflectivity and radial velocity respectively.

SDs of reflectivity and radial velocity are written as functions of observation parameter such as signal to noise ratio (SNR), pulse repitition time, number of pulse, σ_v ([Doviak abd Zrnic , 1993], chapter 6). More realistic way of modeling the sampling error of reflectivity and radial velocity is to add random errors that has Gaussian distribution of SD depends on these parameters. In this study, SNR is assumed as follows:

$$SNR = 10^{\left(\frac{Z-5}{10}\right)} \quad (5)$$

where Z is reflectivity. The uniform noise power with 5 dB is also assumed. From eq. (6.13) and (6.21) of [Doviak abd Zrnic , 1993], SDs of reflectivity and radial velocity are written as follows:

$$SD[V_r] = \{\lambda^2[32\pi^2T^2\rho^2(T)]^{-1}\{M^{-2}[1-\rho^2(T)] \sum_{m=-(M-1)}^{M-1}\rho^2(mT)(M-|m|)+\frac{1}{M}\frac{1}{SNR^2}+ \frac{2}{M}\frac{1}{SNR}[1+\rho(2T)(1/M-1)]\}\}^{\frac{1}{2}} \quad (6)$$

$$SD[Z] = 1+(1+1/SNR)\{ \sum_{m=-(M-1)}^{M-1}\frac{M-|m|}{M^2}\{(1+1/SNR)^{-1}\rho(mT) + (1+SNR)^{-1}\delta_{m,0}\}^2\}^{\frac{1}{2}} \quad (7)$$

where λ is wave length of radar, T and M are pulse repetition time and number of pulse of observation, respectively. $\rho(mT)$ is as follows:

$$\rho(mT) = exp\left[-8(\pi\sigma_v mT_s/\lambda)^2\right] \quad (8)$$

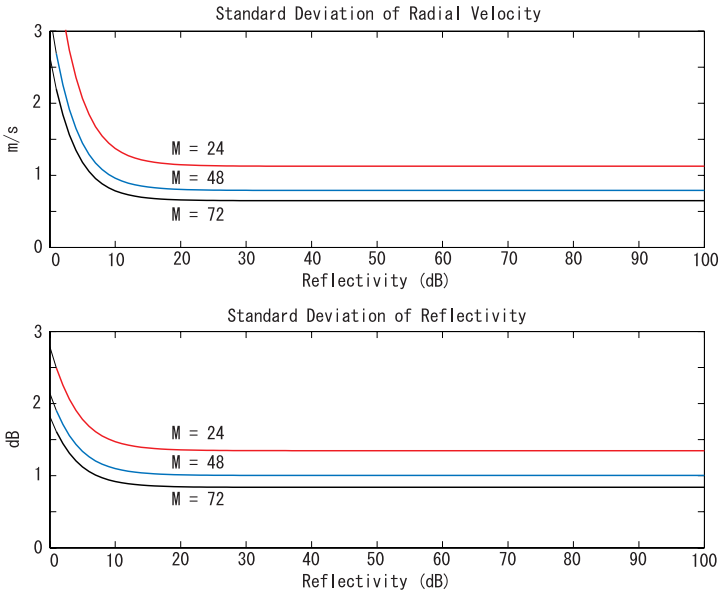

Figure 1: SDs of reflectivity and radial velocity. The red lines are for SDs for M (Number of pulse) = 24, the blue lines are for M = 48, the black lines are for M = 72. As reflectivity and/or M increases, standard deviations of reflectivity and radial velocity become smaller.

σ_v is assumed to be 4 m/s in this study. Estimated SDs of reflectivity and radial velocity using above equations are shown in Figure 1. As reflectivity and/or M increases, both SDs of reflectivity and radial velocity become smaller. In this study, error model depend on M and reflectivity are examined. They are also compared with experiment with uniform SD for M = 24. For uniform values, 1.34 and 1.10 of SDs of reflectivity and radial velocity are used respectively. They are correspond to the values at 100 dB on red curve in Figure 1. In this experiment, reflectivity data more than 10 dBZ are used for data assimilation.

2.3. Experimental design

In this study, the 20 May Del City, Oklahoma supercell storm is simulated using ARPS to serve as the truth for OSSEs. The model domain is 64 $\times$ 64$\times$ 20 km^3 with horizontal spacing of 1 km and 43 vertical levels. The storm is triggered by a thermal bubble placed at the low level of a horizontally homogeneous environment and the model is integrated for two hours. The main storm is located close to the domain at (32,32)km.

The ensemble square root filter scheme is used in this study. Both reflectivity and radial velocity are assimilated from the first analysis cycle. Though all radial velocity observations are used in the analysis, reflectivity observations less than 10 dBZ are not used. The initial ensemble forecast starts at 20 min of model time, and first analysis occurs at 25 min.

The initial ensembles are specified by adding smoothed random perturbations to the initial guess defined by the truth simulation sounding as in TX05, XTD06 and L07. To examine the impact of rapidly updated observation, assimilations of simulated radar observations every 2.5 and 5 min. are conducted.

The radar is located at (-100, 0) km, the southwest corner of the model domain. Two radar beam widths of 2°(PAR) and 1°(WSR-88D) are considered with angular (in azimuth and in elevation) sampling increments of 2°and 1°. Specific configurations of experiments are listed in Table 1. In the experiment names, P and 88D stand for " PAR" and "WSR-88D", M24 or 48 or 72 for "observation with number of pulse of 24 or 48 or 72", C for "using homogeneous SD", U for "using SD depend on M and reflectivity as shown in Figure 1", HF for "radar data assimilation every 2.5 min." as will be explained in the next section.

Table 1: List of Experiments

Experiment	Pulse M	SD of Z	SD of Vr	Time Interval
PM24C	24	1.34	1.10	5
PM24C-HF	24	1.34	1.10	2.5
88DM24C	24	1.34	1.10	5
88DM24C-HF	24	1.34	1.10	2.5
PM48C	48	1.00	0.79	5
PM48C-HF	48	1.00	0.79	2.5
PM72C	72	0.84	0.64	5
88DM48C	48	1.00	0.79	5
88DM48C-HF	48	1.00	0.79	2.5
88DM72C	72	0.84	0.64	5
PM24U	24	ununiform	ununiform	5
PM24U-HF	24	ununiform	ununiform	2.5
88DM24U	24	ununiform	ununiform	5
88DM24U-HF	24	ununiform	ununiform	2.5

3. RESULTS

As shown in Figure 2(a), 88DM24C with 2°beam width and increment shows better performance than PM24C with 1°beam width and sampling increment. PM24C-HF with 2.5 min. assimilation cycles shows better performance than PM24C with 5 min. assimilation cycles. 88D24C-HF also shows better performance than 88DM24C and 88D24C-HF.

There are not remarkable differences between PM24C (observation with 24 pulse), PM48C (48 pulse) and PM72C (72 pulse), nor between PM24C-HF and PM48-HF with 2.5 min. assimilation cycles as shown in Figure 2(b). For 88DM24C (observation with 24 pulse), 88DM48C (48 pulse) and 88DM72C (72 pulse), and 88DM24C-HF and 88DM48-HF, there are not remarkable differences as shown in Figure 2(c).

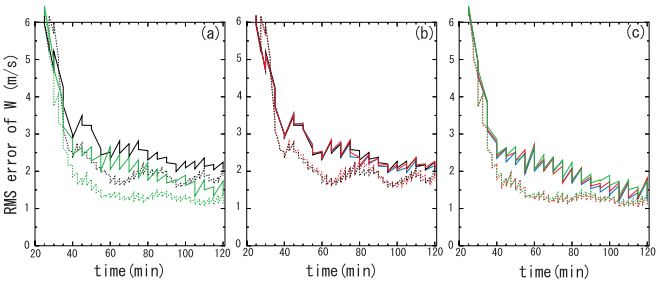

Figure 2: The rms errors of ensemble mean analysis of vertical velocity w, averaged over points at which the true reflectivity is larger than 10 dBZ. The black lines are for experiment PM24C, the dashed black lines are for PM24C-HF, the green lines are for 88DM24C, the dashed green lines are for 88DM24C-HF, the red line in (b) is for PM48C, the dashed red line in (b) is for PM48C-HF, the blue line in (b) is for PM72C, the red line in (c) is for 88DM48C, the dashed red line in (c) is for 88DM48-HF, the blue line in (c) is for 88DM72C.

As shown in Figure 3(a), PM24U added observation errors with SD depend on reflectivity as shown Figure 1 shows worse performance than PM24C with errors with uniform SD of 1.34 for reflectivity and 1.10 for radial velocity. PM24U-HF also shows worse performance than PM24C-HF as shown in Figure 3(b). On the other hand, there are not remarkable differences for WSR-88D, between 88DM24U and 88DM24C, and between 88DM24U-HF and 88DM24C-HF as shown in Figure 3(c).

4. DISCUSSION

The earlier OSSEs assimilating radar data observed various scanning strategies using EnKF are extended to take into account of spatially inhomogeneous and scan-interval-dependent observation error estimates.An error model different from the previously used one is examined for both radar reflectivity and radial velocity data which adds Gaussian-distributed error with SD depend on scanning strategies and reflectivity. This model is more realistic than adding Gaussian-distributed error with uniform SD, and should allow for larger SDs in weaker echo region and less pulse obsrevation.

Though remarkable difference depend on error model is shown for PAR with 2°beam width and sampling increment, the same behavior is not shown for WSR-88D with 1°bem width and sampling increment. Because of the small differences of values of SDs between each reflectivity and pulse number, remarkable difference may not be shown with ARPS ENKF configuration used in this study. Additional experimants using model with higher resolution will be performed to demonstrate positive impact.

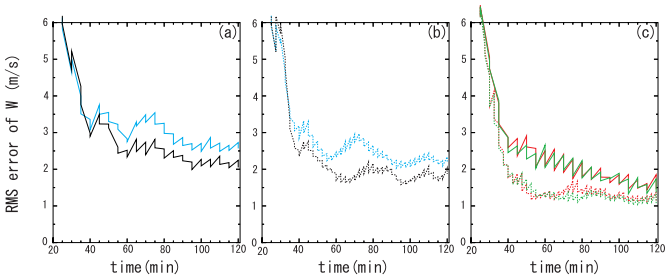

Figure 3: As in Figure 2 but the black line is for experiment PM24C, the blue line is for PM24U, the dashed black line is for PM24C-HF, the dashed blue line is for PM24U-HF, the green line is for 88DM24C, the dashed green line is for 88DM24C-HF, the red line is for 88DM24U, the dashed red line is for 88DM24U-HF.

References

Doviak, R., and D. Zarnic, 1993: *Doppler Radar and Weather Observations*, 2nd ed., *Elsevier, NowYork*.

Jung, Y., M. Xue, G. Zhang, and J. Straka, 2008: Assimilation of simulated polarimetric radar data for a convective storm using ensemble Kalman filter. Part II: Impact of polarimetric data on storm analysis. *Mon. Weather Rev.*, **136**, 1649–1668.

Lei, T., M. Xue, T.-Y. Yu, and M. Teshiba, 2007: Study on the optimal scanning strategies of phased-array radar through ensemble Kalman filter assimilation of simulated data. *33rd Int. Conf. Radar Meeor.,Cairns, Australia, Amer. Meteor. Soc*.P7.1.

Snyder, C, and F. Zhang, 2003: Assimilation of simulated Doppler radar observations with an ensemble Kalman filter. *Mon. Weather Rev.*, **131**, 1663–1677.

Tong, M., and M. Xue, 2005: Ensemble Kalman filter assimilation of Doppler radar data with a compressible nonhydrostatic model: OSS Experiments. *Mon. Weather Rev.*, **133**, 1789–1807.

Wood, V. T., and R. A. Brown, 1997: Effects of radar sampling on single-Doppler velocity signatures of mesocyclones and tornadoes. *Wea. Forecast.*, **12**, 928–938.

Xue, M., M. Tong, and K. K. Droegemeier, 2006: An OSSE framework based on the ensemble squareroot Kalman filter for evaluating impact of data from radar networks on thunderstrom analysis and forecast. *J. Atmos. Oceanic Technol.*, **23**, 46–66.

Yu, T.-Y., M. B. Orescanin, C. D. Curtis, D. S. Zrnic, and D. E. Forsyth, 2007: Beam multiplexing using the pahsed-array weather radar. *J. Atmos. Oceanic Technol.*, **24**, 103–118.

Zhang, F., C. Snyder, and J. Sun, 2004: Impacts of initial estimate and observations on the convective-scale data assimilation with an ensemble Kalman filter. *Mon. Weather Rev.*, **132**, 1238–1253.